

Laser melting of photoluminescent $(Y_{0.92}Eu_{0.08})_2O_3$ films

G. A. Hirata

Department of Mechanical and Aerospace Engineering and Materials Science and Engineering Program, University of California at San Diego, 9500 Gilman Drive, La Jolla, California 92093-0411 and Centro de Ciencias de la Materia Condensada, Universidad Nacional Autonoma de Mexico, Km. 103 Carretera Ensenada-Tijuana, Ensenada, B.C., 22860, Mexico

J. McKittrick^{a)}

Department of Mechanical and Aerospace Engineering and Materials Science and Engineering Program, University of California at San Diego, 9500 Gilman Drive, La Jolla, California 92093-0411

M. Trkula

Materials Science and Technology Division, Los Alamos National Laboratory, Los Alamos, New Mexico 87545

J. Mourant and R. Sze

Chemical Science and Technology Division, Los Alamos National Laboratory, Los Alamos, New Mexico 87545

(Received 23 January 2001; accepted for publication 24 July 2001)

Fluorescent red-emitting $(Y_{0.92}Eu_{0.08})_2O_3$ films were deposited on sapphire substrates by the metallorganic chemical vapor deposition technique. The films were weakly luminescent in the as-deposited condition. The as-deposited films were composed of nanocrystals embedded in columnar grains. A KrF laser with ultraviolet ($\lambda=248$ nm) pulses at a fluence level between 0.9 and 2.3 J/cm² was applied to different regions of the film. Increasing the energy fluence density initially increased the photoluminescence intensity but decreased it at the highest level. Transmission and scanning electron microscopy verified that surface melting and ablation occurred at all fluence levels. Computational modeling of the laser melting and ablation process predicted that a significant fraction of the film is removed by ablation at the highest fluence levels, thereby decreasing the photoluminescence intensity of the films due to the significant amount of material removed.

© 2001 American Institute of Physics. [DOI: 10.1063/1.1404428]

I. INTRODUCTION

Surface modification of materials can be achieved by the absorption of an intense laser pulse to obtain materials not accessible by other processing techniques. When a high intensity ultraviolet (UV) pulsed photon beam is absorbed by the surface, the energy is transferred to heat in less than 1 ps. This can be used to melt and subsequently solidify the irradiated area and/or to simply alter the surface structure of the solid. Laser surface modification has been used to fabricate novel microstructures and alloys,¹ obtain a micromachined morphology,² enhance chemical reactions and modify the surface chemistry of novel nanostructured thin films.^{3,4} Pulsed excimer lasers have been used to crystallize amorphous ferroelectric films^{5,6} and amorphous semiconductors⁷⁻¹⁰ and induce grain growth in silicon through melting and solidification.¹¹ The improvement of luminescent intensity in red-emitting luminescent films *via* laser melting has also been investigated.¹²

Luminescent thin films are materials that emit photons (IR-UV) when excited by an external energy source, such as an electric field, photons or electrons. These films have application for flat panel displays and as biological, chemical and thermal sensors. Several articles been published on the

deposition, processing, and optoelectronic and/or structural characterization of oxide luminescent films, including $(Zn_{1-x}Mn_x)_2SiO_4$,¹³ $(Y_{1-x}Eu_x)_2O_3$,¹⁴ and $Zn_{1-x}O$.¹⁵ The as-deposited films are nanocrystalline and weakly luminescent. However, highly crystalline, large grain size films are required to maximize the luminescence emission intensity.^{13,15} This occurs only under postdeposition annealing at high temperatures (>1000 °C), thereby restricting the use of rapid thermal annealing or conventional furnace annealing due to substrate/film interactions.^{12,16} In addition, substrates are limited to quartz or sapphire, undesirable substrates for commercial applications.

Synthesis of luminescent thin films has been performed by several methods such as rf magnetron sputtering,^{17,18} metallorganic chemical vapor deposition (MOCVD)¹⁹⁻²¹ and pulsed laser deposition.²²⁻²⁴ The fabrication processes usually require substrate temperatures >500 °C to produce (poly)crystalline films that are subsequently subjected to postdeposition, high temperature annealing.

Decreasing the fabrication temperature and time for film deposition has been the goal for many scientists. Laser processing of luminescent thin films has many advantages over standard heat treatment methods. The substrate is not exposed to elevated temperatures, the processing times and impurity diffusion are reduced and laser treatment is an extremely fast clean process, free of heater elements and

^{a)}Author to whom correspondence should be addressed.

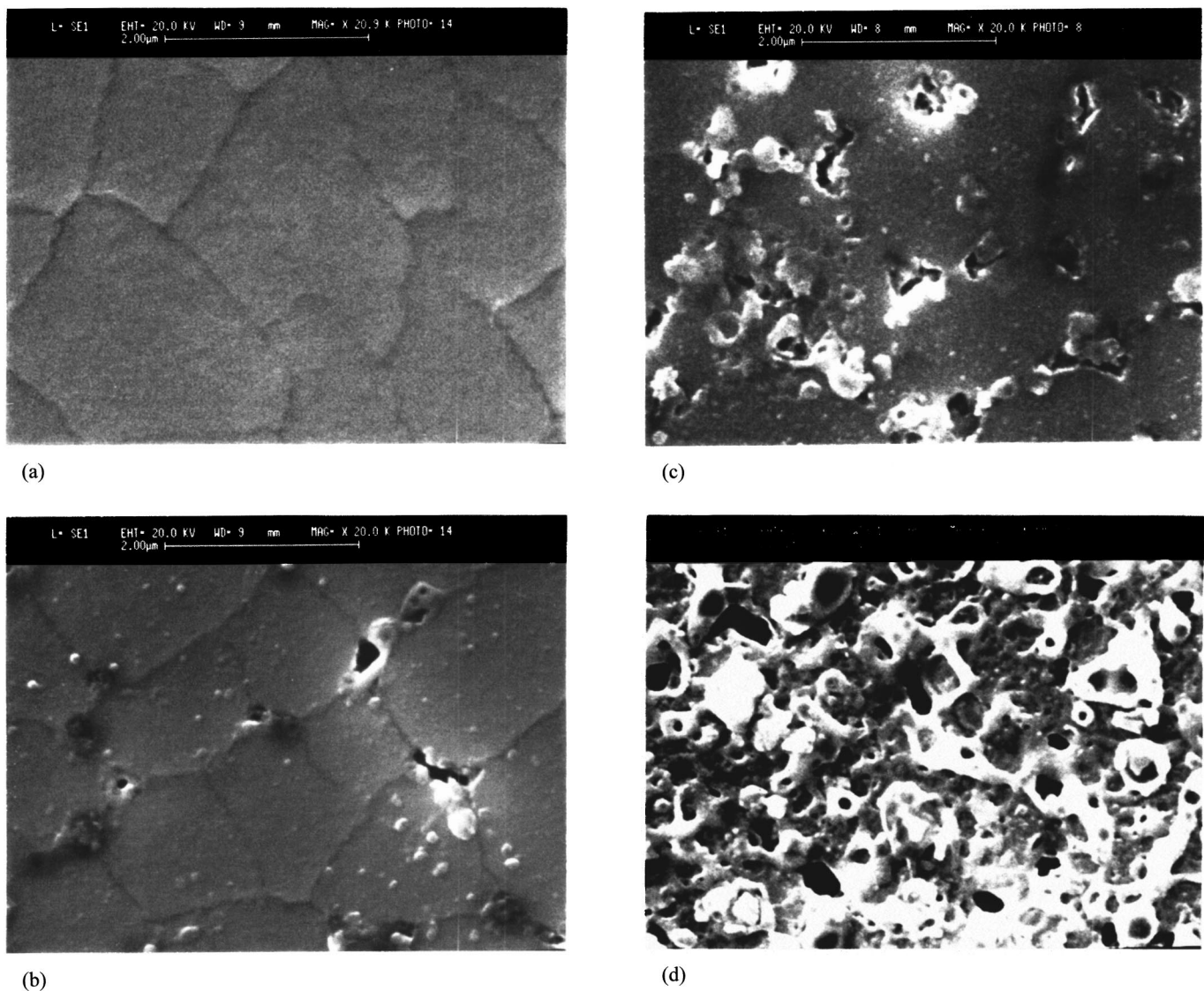


FIG. 1. SEM micrographs of the (a) as-deposited $(Y_{1-x}Eu_x)_2O_3$, (b) after one pulse at 0.9 J/cm^2 , (c) after one pulse at 1.4 J/cm^2 and (d) after one pulse at 2.3 J/cm^2 .

contaminants usually found in conventional furnaces. Additionally, the substrates would not have to withstand high temperatures, thereby opening other materials choices, including polymers.

In a previous article we reported that one laser pulse at a fluence of 1.02 J/cm^2 was enough to melt the surface of a $(Y_{1-x}Eu_x)_2O_3$ film and repeated pulses caused ablation of the material. The laser processing melted the as-deposited film, which smoothed and densified the film. Moreover, the photoluminescence (PL) emission intensity of the laser melted $(Y_{1-x}Eu_x)_2O_3$ films was improved by 122% over that of the as-deposited film.¹²

The objective of this work was to apply a high energy (UV) laser pulse at different fluence densities to films of $(Y_{1-x}Eu_x)_2O_3$ to examine the microstructural and luminescence properties of the treatment. Additionally, it was the goal to compare the physical observations to a computational model of the laser melting and ablation process.

II. EXPERIMENTAL TECHNIQUES

$(Y_{1-x}Eu_x)_2O_3$ films were grown by MOCVD on heated sapphire under similar conditions as described in a previous article.¹⁴ A Lambda-Physik KrF excimer ($\lambda=248 \text{ nm}$) laser with 25 ns pulse width was applied to the surface of the as-deposited films. A homogenizer was used to produce a rectangular beam ($6 \times 9 \text{ mm}^2$) resulting in an energy fluence density that was adjusted to range between 0.9 and 2.3 J/cm^2 . Different regions of the film were used for each application of the laser. The morphology of the as-deposited and laser-irradiated samples was analyzed with a scanning electron microscope (SEM) operated at 20 kV. Cross-sectional analysis was performed utilizing a field emission transmission electron microscope (TEM) operated at 300 kV. The TEM cross-sectioned samples were prepared by gluing two samples together face to face (to protect the area of interest and at the same time to increase the number density

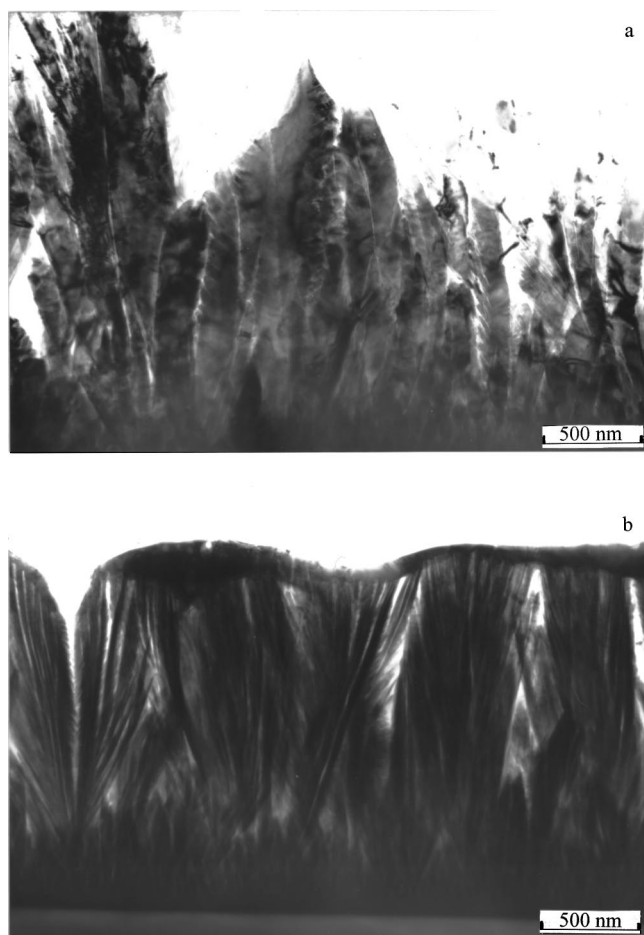


FIG. 2. TEM cross-sectional micrographs of (a) an as-deposited $(Y_{1-x}Eu_x)_2O_3$ film and (b) a laser-melted area with a fluence density of 1.4 J/cm^2 .

of crystals in the thinned area). PL measurements were taken under ambient conditions by exciting the as-deposited and laser-melted regions with $\lambda=250 \text{ nm}$ UV photons and then collecting the emission spectra (in the range of $300\text{--}700 \text{ nm}$) in transmission mode. A $250 \mu\text{m}$ fiberoptic cable connected to an Acton Research spectrograph attached to a thermoelectrically cooled Princeton Instruments charge coupled device camera collected the spectra.

The thermal profile, melt and ablation depths as a function of time were calculated using a finite difference simulation program called SLIM, the simulation of laser interaction with materials.²⁵ The output to this program is the solution to a one-dimensional heat flow problem. This is a reasonable approximation due to the short pulse duration of the laser that yields thermal gradients perpendicular to the surface orders of magnitude higher than the gradients parallel to the surface. The input data to the program are: thickness of the film, melting and vaporization temperature of the film, temperature dependent thermal conductivity of the film and substrate, temperature dependent heat capacity of the film and substrate, temperature dependent reflectivity (solid and liquid) of the film, heats of melting and vaporization of the film, and adsorption coefficient for the solid, liquid and vapor. The laser energy pulse was input as a square pulse with a 25 nm width. The energy was varied for each fluence level. The film

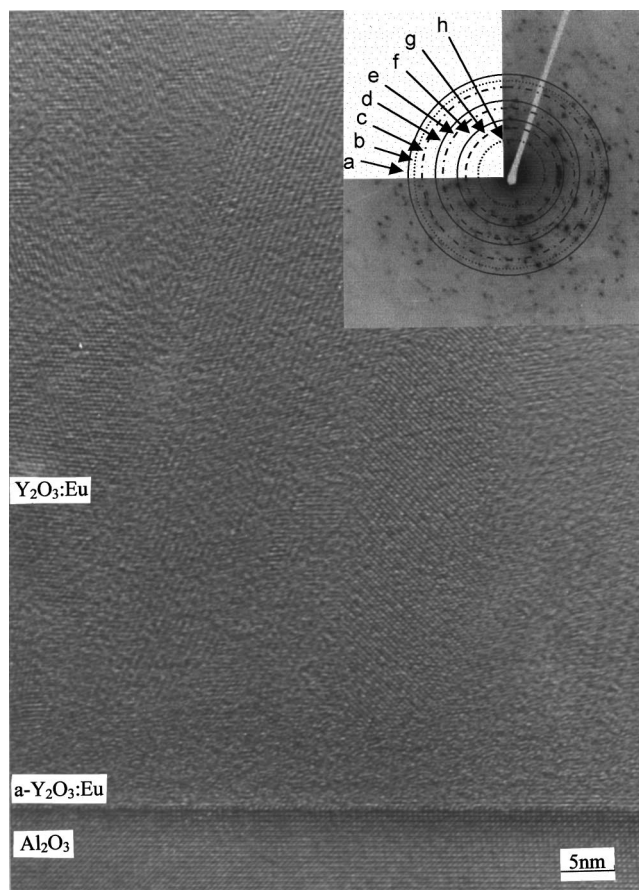


FIG. 3. Lattice fringe image of the interface between the as-synthesized $(Y_{1-x}Eu_x)_2O_3$ film and the sapphire substrate.

and substrate were considered semi-infinite, the number of nodes was 100, the time iteration interval was 40 ps and the program was allowed to melt the substrate, if sufficiently high temperatures were reached.

III. RESULTS AND DISCUSSION

The as-deposited films were weakly luminescent with the characteristic red/orange emission of $(Y_{1-x}Eu_x)_2O_3$. The composition was previously determined to be $x=0.08$ by Rutherford backscattering.¹² Figure 1(a) shows the SEM micrograph of an as-deposited film. The surface appears smooth and has a grain size of $\sim 2\text{--}3 \mu\text{m}$ composed of nanometer sized crystallites. Figure 1(b) shows the film after the application of one laser pulse at 0.9 J/cm^2 . The micrograph shows there was some thermal cracking and melting as observed at the grain boundaries. Porosity has also been induced at the grain boundaries from laser ablation, as the ejecta can be observed on the surface around the pores. As shown in Fig. 1(c), after one pulse at 1.4 J/cm^2 , a larger fraction of melting is observed. The grain boundaries are no longer evident and the nanocrystallites have increased in size and spheroidized. It appears that a significant fraction of the surface has melted. An increase in the amount of ablated material is also detected. After one pulse at 2.3 J/cm^2 , the

surface is considerably rougher than at the lower fluence levels and large solidification voids can be observed, as shown in Fig. 1(d).

Figure 2(a) shows a cross-sectional TEM view corresponding to an as-deposited film. The film is composed of columnar crystallites of the order of 0.2–0.3 μm width and $\sim 2 \mu\text{m}$ long (the thickness of the film). It is seen that some of the columnar grains grow independently, resulting in a small separation between crystallites. Figure 2(b) shows a TEM micrograph of the laser-melted area that was exposed to a fluence density of 1.4 J/cm^2 . It is clearly observed that the columnar “peaked” surface in Fig. 2(a) has disappeared and the film is smoother and denser. The laser-melted areas appear to retain some growth orientation due to the unidirectional solidification. The grain width is smaller, indicating that the film solidified rapidly.

Figure 3 shows a TEM lattice fringe image of the interface between the as-synthesized film and the sapphire substrate. It can be seen that the columnar grains are grown after a quasicrystalline layer of $(\text{Y}_{1-x}\text{Eu}_x)_2\text{O}_3$ is formed at the initial stage of the MOCVD deposition. The quasi-crystalline region is either amorphous (crystallite size $< 0.5 \text{ nm}$) or corresponds to crystallites that are oriented, with respect to the electron beam, in such a way that no Bragg reflection occurs for this particular sample orientation. Lattice fringes of the film show different crystallographic directions, indicating the film is polycrystalline. In corroboration, the diffraction pattern from this area shown as an inset to Fig. 4 also shows the polycrystalline characteristics of the film. The ring-type diffraction pattern with certain intensity enhancement along the rings indicates that the film is composed of Y_2O_3 with some preferred growth directions. The diffraction rings were identified and were matched to both cubic²⁶ and monoclinic²⁷ Y_2O_3 . Monoclinic Y_2O_3 is a metastable phase, thought to be stabilized under ambient conditions by the Gibbs–Thompson effect as nanocrystalline particles.²⁸ Rings a–c match the planar distances given for the cubic, whereas rings d–f correspond to the monoclinic structure.

PL measurements of the laser processed films at different fluences are shown in Fig. 4. The characteristic 611 nm feature of cubic $(\text{Y}_{1-x}\text{Eu}_x)_2\text{O}_3$ is seen along with the 628 nm feature identified as monoclinic $(\text{Y}_{1-x}\text{Eu}_x)_2\text{O}_3$.²⁸ In the as-deposited state, the emission intensity is very weak, and the

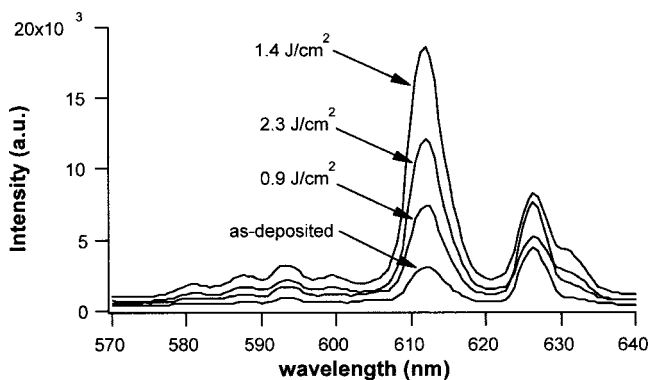


FIG. 4. Photoluminescent emission spectra of the as-deposited and laser processed $(\text{Y}_{1-x}\text{Eu}_x)_2\text{O}_3$ film.

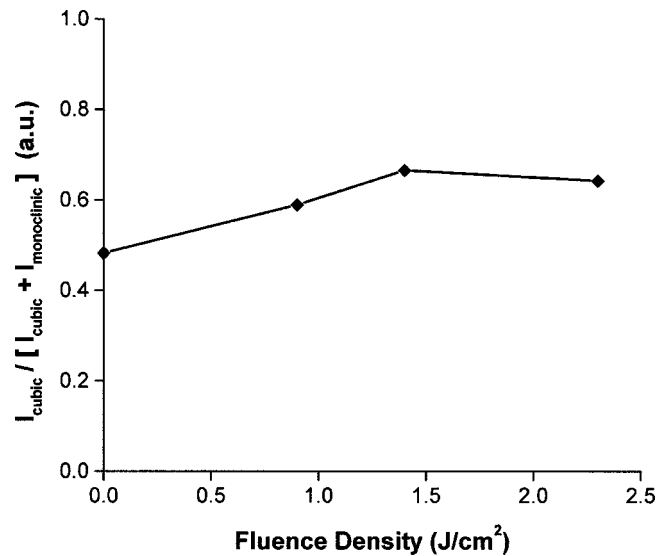


FIG. 5. Change of the ratio cubic/monoclinic luminescent intensity in $(\text{Y}_{1-x}\text{Eu}_x)_2\text{O}_3$ films with laser irradiation.

monoclinic feature is more intense than the one for the cubic structure. After the application of 0.9 J/cm^2 , the emission intensity increased for both the cubic and monoclinic features. The highest emission intensity occurred for 1.4 J/cm^2 , where the cubic feature is significantly higher than the monoclinic feature. An increase to 2.3 J/cm^2 decreased the emission intensity, which was unexpected, since the emission intensity was initially increasing with higher fluence levels. Laser irradiation increased photoluminescence at 611 nm (cubic contribution). The increase in the surface temperature caused melting of the Y_2O_3 film and it converts part of the monoclinic into the cubic phase because cubic is the stable phase at high temperatures.^{12,14} The change of the ratio of cubic/monoclinic luminescent intensity with laser irradiation is illustrated in Fig. 5. It can be observed that the luminescence contribution of the cubic phase is improved as the fluence density is increased.

Figure 6 shows the calculated melt and ablation depth profiles by the SLIM program for three energy fluence lev-

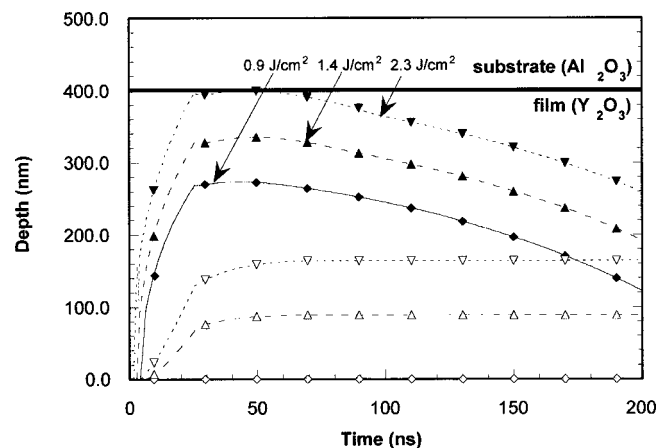


FIG. 6. Calculated melt and ablation depth profiles by the SLIM program for different fluence levels. Solid symbols represent the melt depth, open symbols represent ablation depth.

TABLE I. Input parameters for the SLIM program. Data taken from Ref. 29.

Property	Al ₂ O ₃ (substrate)	Y ₂ O ₃ (film)
Melting temperature (K)	2323	2693
Evaporation temperature (K)	3253	4603
Heat of melting (J/cm ³)	4400	2220
Heat of vaporization (J/cm ³)	18 912	43 499
Thermal conductivity (W/cm K)		
Solid	48.6 $T^{-0.894}$	6.86 $T^{-0.823}$
Liquid	0.0476	0.0103
Heat capacity (J/cm ³ K)		
Solid	$7.15 \times 10^{-4}T - 1.18 \times 10^5 T^{-2}$	$7.29 \times 10^{-4}T$
Liquid	+4.26	$-1.96 \times 10^4 T^{-2} + 2.31$
Absorption coefficient (cm ⁻¹)	5.9	4.27
Solid	5×10^4	5×10^4
Liquid	5×10^4	5×10^4
Reflectivity (J/cm ³ K)		
Solid		0.2
Liquid		0.2

els: 0.9, 1.4 and 2.3 J/cm². The input data²⁹ are given in Table I. A 400-nm-thick film was modeled. The melt depth (solid) symbols and ablation depth (open symbols) are shown as a function of time. A fluence of 0.9 J/cm² shows a melt depth maximum to be 280 nm. This increases to 330 nm at 1.4 J/cm² and to 400 nm at 2.3 J/cm². This indicates that melting should have been observed for all the fluence levels used in this experiment, and is corroborated by the SEM micrographs shown in Fig. 1. The ablated depths are shown as the open symbols. Negligible ablation occurs at a fluence density of 0.9 J/cm². At 1.4 J/cm², almost 80 nm of the film was removed while at 2.3 J/cm², approximately 150 nm of the film was removed. As the volume of material melted increases, the PL emission intensity increases due to an increase in density of the solidified regions and the reduction of nanocrystallites. However, as the melted volume increases, the amount of material removed by ablation also increases. Thus, there is a trade-off between maximizing the PL intensity by increasing the volume of melted material and decreasing the PL intensity by material ablation.

IV. CONCLUSIONS

Luminescent films of (Y_{0.92}Eu_{0.08})₂O₃ were synthesized by chemical vapor deposition from organometallic precursors onto heated sapphire substrates. Laser melting of the films was achieved with a 248 nm KrF excimer laser with a pulse width of 25 ns and at fluences between 0.9 and 2.3 J/cm². The laser pulse melted the as-deposited film that increased the photoluminescent emission intensity. The photoluminescent emission intensity increased with higher fluence levels, however significant ablation occurred at the highest fluence level. Direct observations with transmission and scanning electron microscopy performed on films verified that melting and ablation occurred at all fluence levels. Computational modeling of the laser melting and ablation process predicted that a significant fraction of the film is removed by

ablation at the highest fluence levels, thereby decreasing the photoluminescence intensity of the films at the highest fluence level.

ACKNOWLEDGMENTS

The authors would like to thank Ross Muenchausen at LANL for helping with the SLIM calculations. One of us (G. A. H.) acknowledges partial support from CoNaCyT and DGAPA-UNAM. This work was conducted under the auspices of the U.S. Department of Energy, supported (in part) by funds provided by the University of California for the conduct of discretionary research by Los Alamos National Laboratory under project CULAR and the Visiting Scholar Program and through the Phosphor Technology Center of Excellence, DARPA Grant No. MDA972-93-1-0030.

- ¹R. Serna, A. Blasco, T. Missana, J. Solis, C. N. Afonso, A. Rodriguez, and M. F. da Silva, *Appl. Phys. Lett.* **68**, 1781 (1996).
- ²T. Sameshima, *Jpn. J. Appl. Phys., Part 2* **32**, L1485 (1993).
- ³L. Calcagnile, M. G. Grimaldi, and P. Baeri, *J. Appl. Phys.* **76**, 1833 (1994).
- ⁴K. M. Kramer and M. O. Thompson, *J. Appl. Phys.* **79**, 4118 (1996).
- ⁵S. B. Xiong, Z. M. Ye, J. M. Liu, A. D. Li, C.-Y. Lin, S. Y. Chen, X. L. Guo, and Z. G. Liu, *Appl. Surf. Sci.* **109/110**, 124 (1997).
- ⁶J. S. Zhu, X. M. Lu, X. Tiu, and Z. Yang, *Mater. Res. Soc. Symp. Proc.* **397**, 413 (1995).
- ⁷C. N. Afonso, J. Solis, F. Vega, J. Siegel, and W. Szyszko, *Appl. Surf. Sci.* **109/110**, 20 (1997).
- ⁸M. D. Efremov, V. V. Bolotov, V. A. Volodin, L. E. Fedina, and E. A. Lipatnikov, *J. Phys.: Condens. Matter* **8**, 273 (1996).
- ⁹J. S. Im, H. J. Kim, and M. O. Thompson, *Appl. Phys. Lett.* **63**, 1969 (1993).
- ¹⁰P. M. Smith, S. Lombardo, M. J. Uttormark, S. J. Cook, and M. O. Thompson, *Mater. Res. Soc. Symp. Proc.* **202**, 603 (1991).
- ¹¹R. Ishihara and P. Ch. van der Wilt, *Jpn. J. Appl. Phys., Part 2* **37**, L15 (1998).
- ¹²J. McKittrick, G. A. Hirata, C. Bacalski, R. Sze, J. Mourant, K. M. Hubbard, M. Trkula, and T. R. Gosnell, *J. Mater. Res.* **13**, 3019 (1998).
- ¹³H. P. Maruska, T. Parodos, N. M. Kalkhouraud, and W. D. Halverson, *Mater. Res. Soc. Symp. Proc.* **345**, 269 (1994).
- ¹⁴G. A. Hirata, J. McKittrick, M. Avalos-Borja, J. M. Siqueiros, and D. Devlin, *Appl. Surf. Sci.* **113/114**, 509 (1997).

- ¹⁵R. O. Petersen, *Inf. Disp.* **13**, 22 (1997).
- ¹⁶G. A. Hirata, O. A. Lopez, L. E. Shea, J. McKittrick, T. Cheeks, J. Y. Yi, J. Siqueiros, and M. Avalos, *J. Vac. Sci. Technol. A* **14**, 1694 (1996).
- ¹⁷X. Ouyang and A. H. Kitai, *J. Appl. Phys.* **79**, 3229 (1996).
- ¹⁸I. J. Hsieh, K. T. Chu, C. F. Yu, and M. S. Feng, *J. Appl. Phys.* **76**, 3735 (1994).
- ¹⁹J. P. Dismukes, J. Kane, B. Binggeli, and H. P. Schweizer, in *Chemical Vapor Deposition: Fourth International Conference*, edited by G. F. Wakefield and J. M. Blocher (The Electrochemical Society, Princeton, NJ, 1973).
- ²⁰G. A. West and K. W. Beeson, *J. Mater. Sci.* **5**, 1573 (1990).
- ²¹J. McKittrick, C. F. Bacalski, G. A. Hirata, K. M. Hubbard, S. G. Pattillo, K. V. Salazar, and M. Trkula, *J. Am. Ceram. Soc.* **83**, 1241 (2000).
- ²²G. A. Hirata, J. McKittrick, M. Avalos-Borja, J. M. Siqueiros, and D. Devlin, *Appl. Surf. Sci.* **113/114**, 509 (1997).
- ²³S. L. Jones, D. Kumar, R. K. Singh, and P. H. Holloway, *Appl. Phys. Lett.* **71**, 404 (1997).
- ²⁴K. G. Cho, D. Kumar, D. G. Lee, S. L. Jones, P. H. Holloway, and R. K. Singh, *Appl. Phys. Lett.* **71**, 3335 (1997).
- ²⁵SLIM, simulation of laser interactions with materials, R. Singh and J. Viatella, University of Florida, Gainesville, FL 32611-2066.
- ²⁶JCPDS No. 41-1105, Joint Committee on Powder Diffraction Standards: International Center for Diffraction Data (ICDD), 12 Campus Blvd., Newtown Square, PA 19073-3273.
- ²⁷JCPDS No. 44-0399, Joint Committee on Powder Diffraction Standards: International Center for Diffraction Data (ICDD), 12 Campus Blvd., Newtown Square, PA 19073-3273.
- ²⁸H. Eilers and B. M. Tissue, *Chem. Phys. Lett.* **251**, 74 (1996).
- ²⁹G. V. Samsonov, *The Oxide Handbook*, translated from the Russian by Robert K. Johnston (IFI/Plenum, New York, 1982).